Direct-current Energy Generators from Polypyrrole-coated Fabric/Metal Schottky Diodes with Considerably Improved Output

Wenyu Wang[a,1], Xing Han[a,1], Jiarong Niu[a], Xin Jin[b,*], Hongxia Wang[c], Hao Shao[c], Tong Lin[c,*]

a State Key Laboratory of Separation Membranes and Membrane Processes, School of Textile Science and Engineering, Tiangong University, Tianjin 300387, P. R. China.
b State Key Laboratory of Separation Membranes and Membrane Processes, School of Materials Science and Engineering, Tiangong University, Tianjin 300387, P. R. China
c Institute for Frontier Materials, Deakin University, Geelong, Victoria 3216, Australia

[1] Both authors contributed equally to the manuscript.

Corresponding authors' emails: jinxin29@126.com; tong.lin@deakin.edu.au

Electronic Supplementary Information

The preparation of PPy-coated Au:

The Au-coated PET film was used as a substrate. PPy was electrodeposited on the gold surface using a three-electrode electrochemical method, in which a platinum plate (1 cm × 1 cm) and an Ag/AgCl standard electrode were used as the counter and reference electrodes, respectively. The deposition was carried out in a solution containing 0.15 M sodium dodecyl sulfate (SDS) and 0.15 M pyrrole. The electrodeposition potential was set at 0.8 V for 120 s (CHI 660E electrochemical workstation). The resulting film was rinsed with deionized water and dried at 60 ℃.

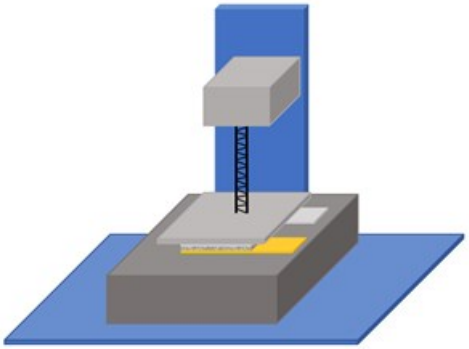

Fig. S1 Schematic diagram to show the testing setup.

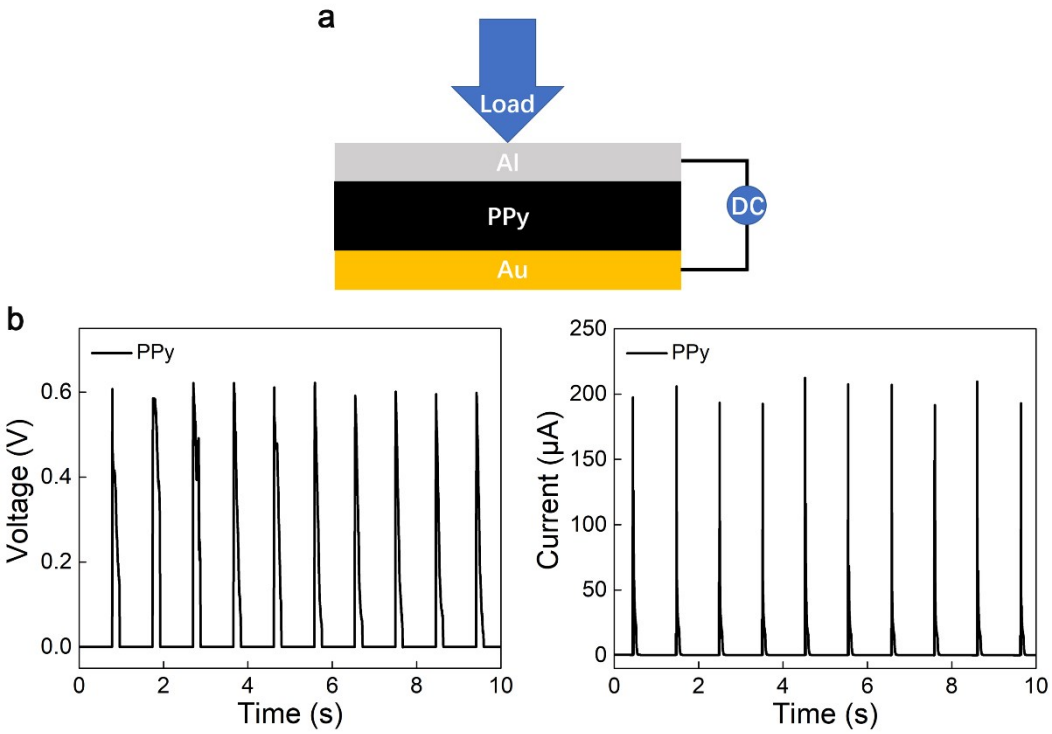

Fig. S2 (a) Schematic diagram of the Au/PPy/Al device, (b) voltage and current outputs of the Au/PPy plate/Al device under repeated compressive deformation.

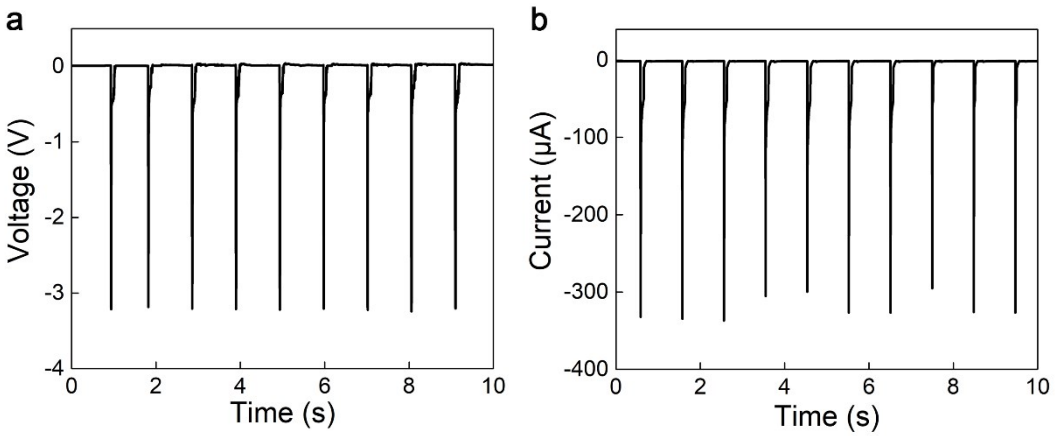

Fig. S3 (a) Voltage and (b) current outputs of the Al/PPy-coated fabric/Au device at the reserve connection condition.

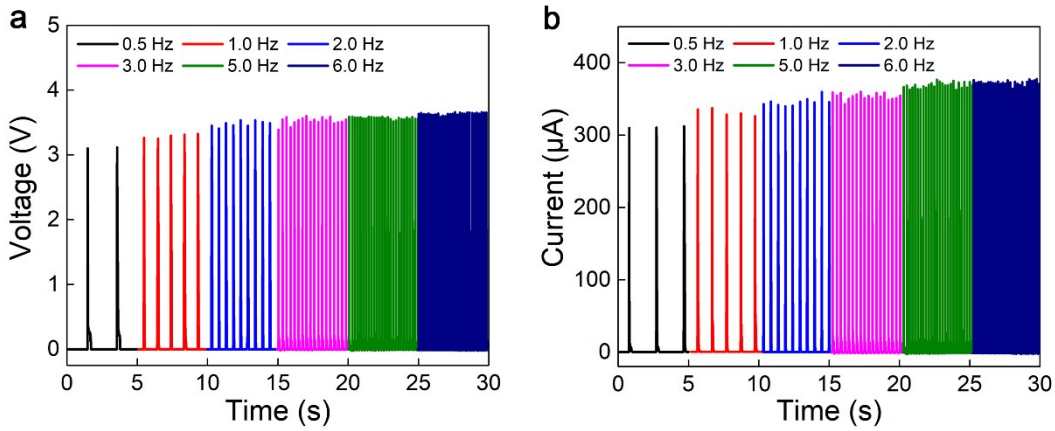

Fig. S4 (a) Voltage and (b) current outputs of the Al/PPy-coated fabric/Au device at different frequencies.

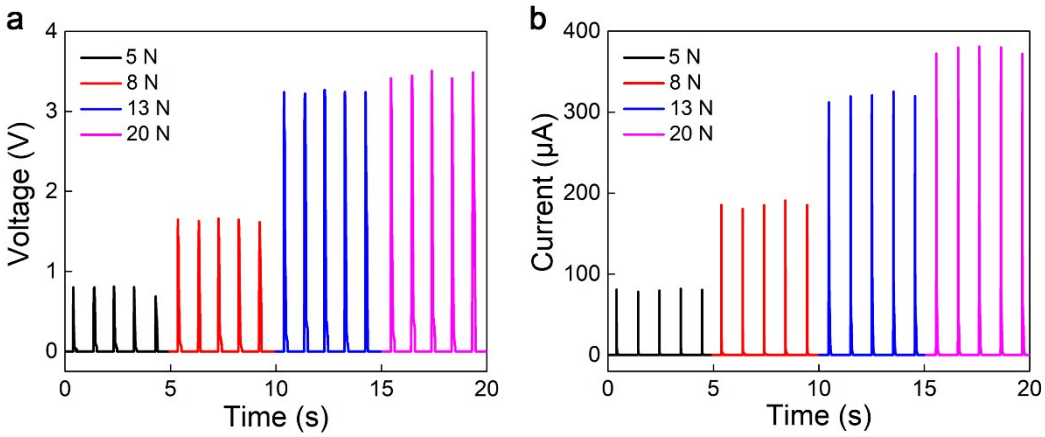

Fig. S5 (a) Voltage and (b) current outputs of the Al/PPy-coated fabric/Au device at different forces.

With increasing the impact force from 5 N to 8 N and 13 N, the voltage output increased from 0.78 V to 1.64 V and 3.24 V, while when further increasing the force from 13 N to 20 N, the voltage increases at a lower extent, from 3.24 V to 3.45 V. The current output change in a similar trend. This changing trend can be explained by the influence of impact force on the compressive deformation of the fabric. Since the electrical generation is mainly contributed by the triboelectric effect. The electric output is mainly dependent on the fiber-electrode contact caused by compression. A larger contact area results in larger outputs. When increasing the impact force, the fabric can be pressed to a denser state, which leads to a larger contact area, until it reaches the fully compacted state in which further increasing the force will not cause an increase in the contact area.

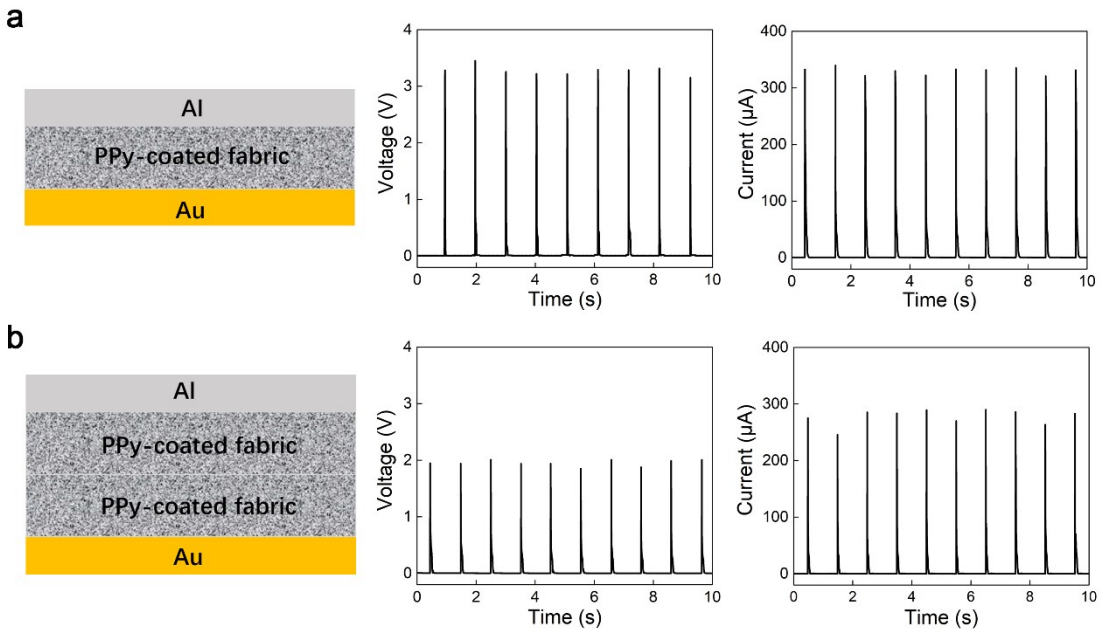

Fig. S6 Electrical outputs of Al/PPy-coated fabric/Au device made of (a) single PPy-coated fabric and (b) two layers of PPy-coated fabrics.

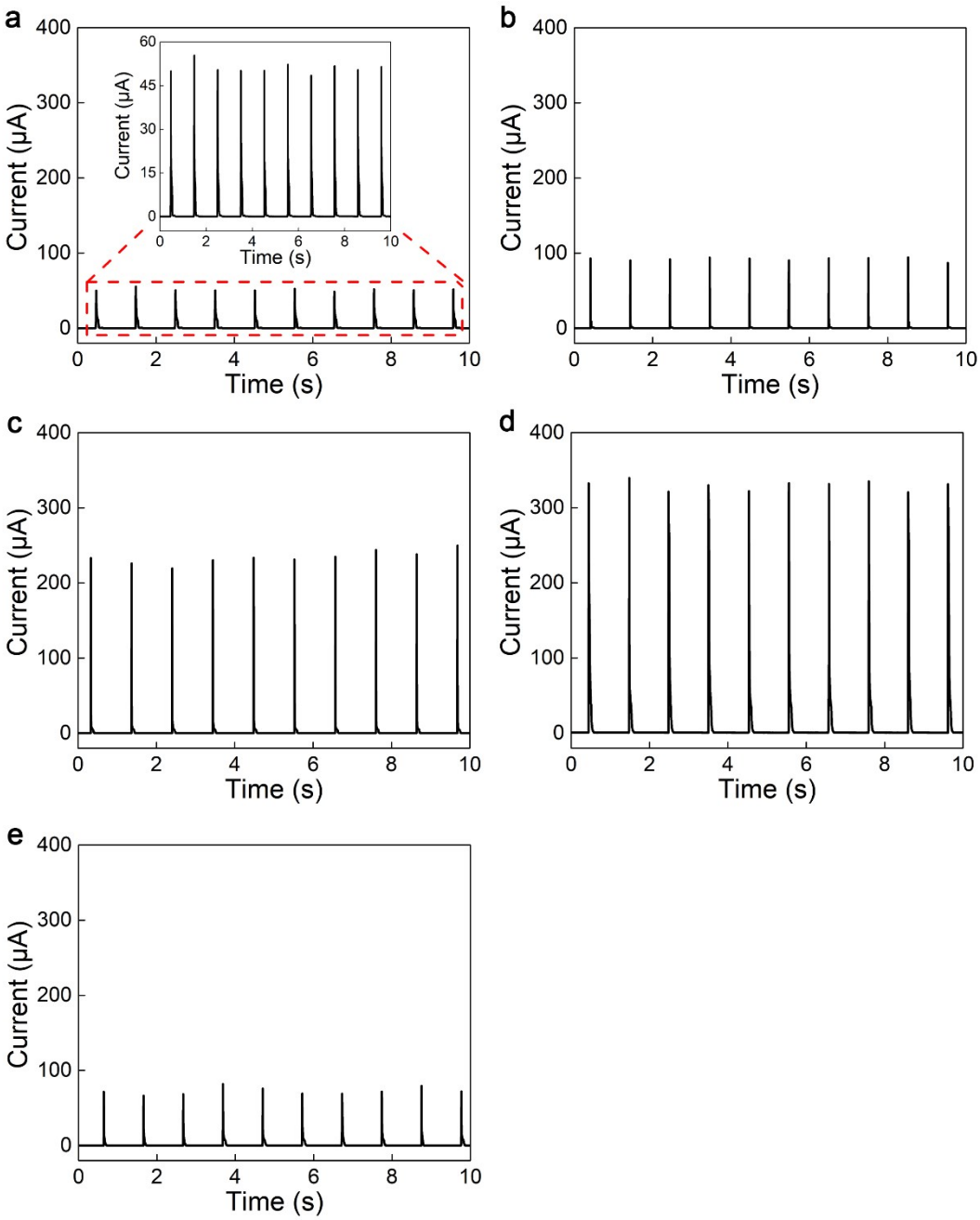

Fig. S7 Current outputs of the devices made of the PPy-coated fabrics with different PPy loadings (a) 2.70 mg/cm^2, (b) 4.06 mg/cm^2, (c) 4.22 mg/cm^2, (d) 6.36 mg/cm^2, and (e) 6.44 mg/cm^2.

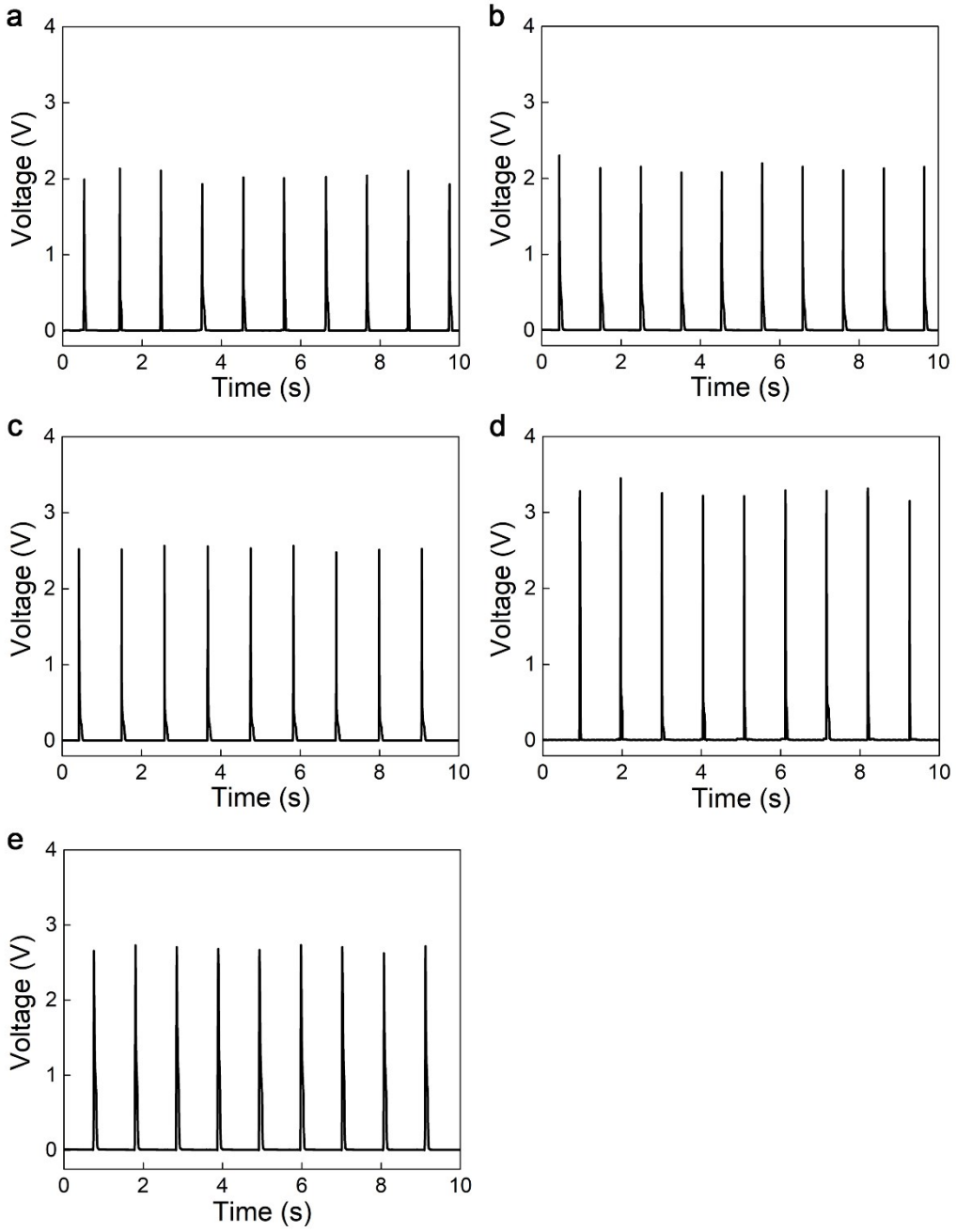

Fig. S8 Voltage outputs of the devices from the PPy-coated fabrics with different PPy loadings (a) 2.70 mg/cm^2, (b) 4.06 mg/cm^2, (c) 4.22 mg/cm^2, (d) 6.36 mg/cm^2, and (e) 6.44 mg/cm^2.

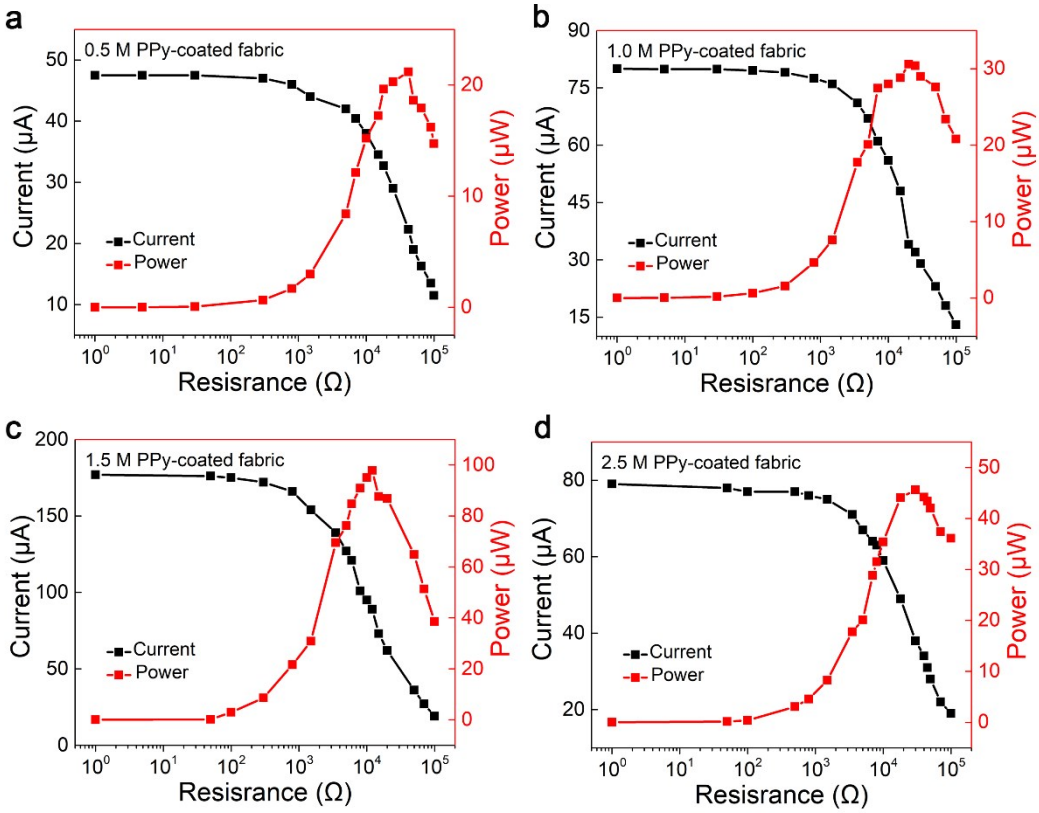

Fig. S9 Dependence of the current outputs and power on external resistance for the Al/PPy-coated fabric/Au device made of the PPy-coated fabric with different PPy loadings (a) 2.70 mg/cm^2, (b) 4.06 mg/cm^2, (c) 4.22 mg/cm^2, (d) 6.36 mg/cm^2, and (e) 6.44 mg/cm^2.

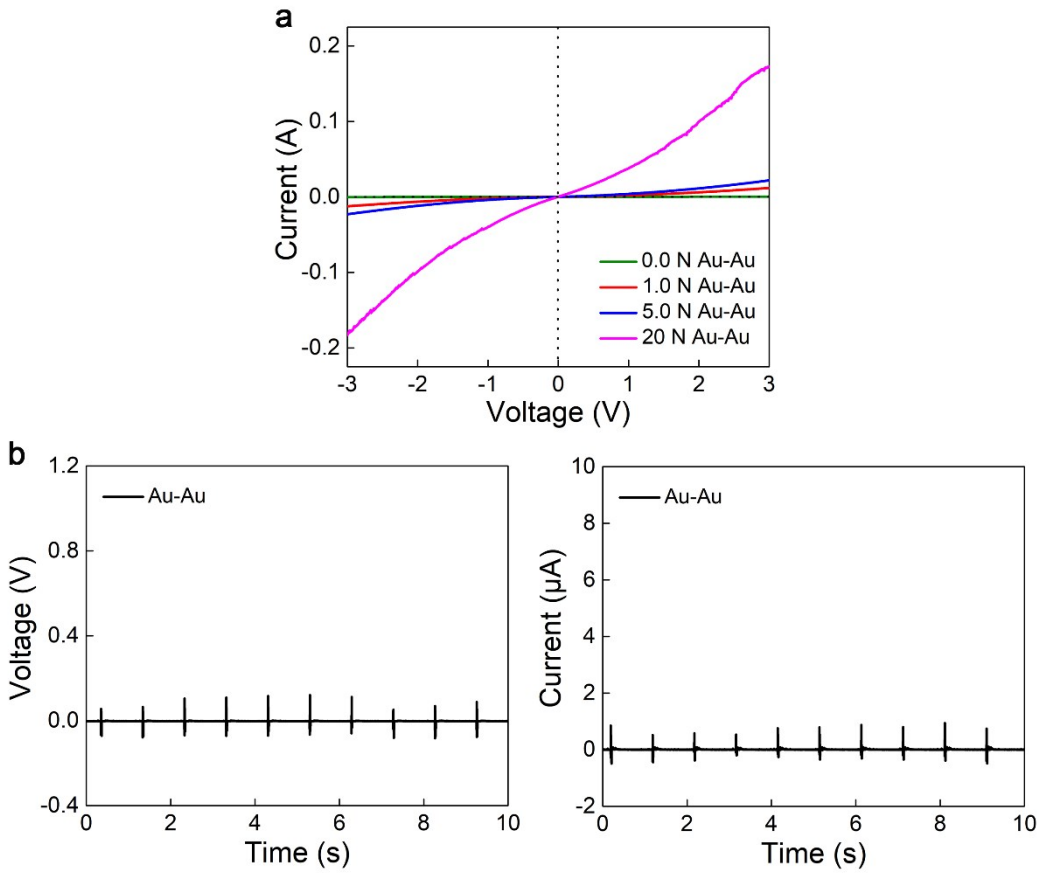

Fig. S10 (a) I-V characteristics of Au/PPy-coated fabric/Au under different forces, (b) voltage and current outputs of the Au/PPy-coated fabric/Au device.

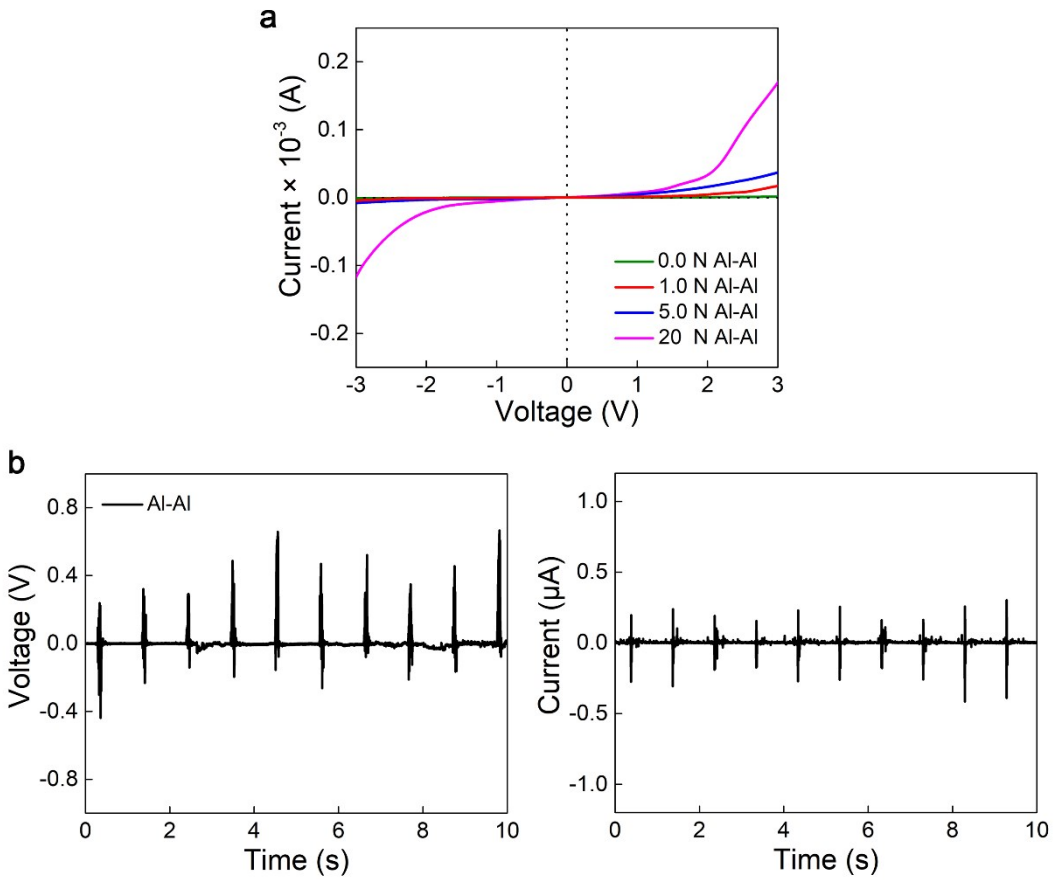

Fig. S11 (a) I-V characteristics of Al/PPy-coated fabric/Al at different forces, (b) voltage and current outputs of the Al/PPy-coated fabric/Al device.

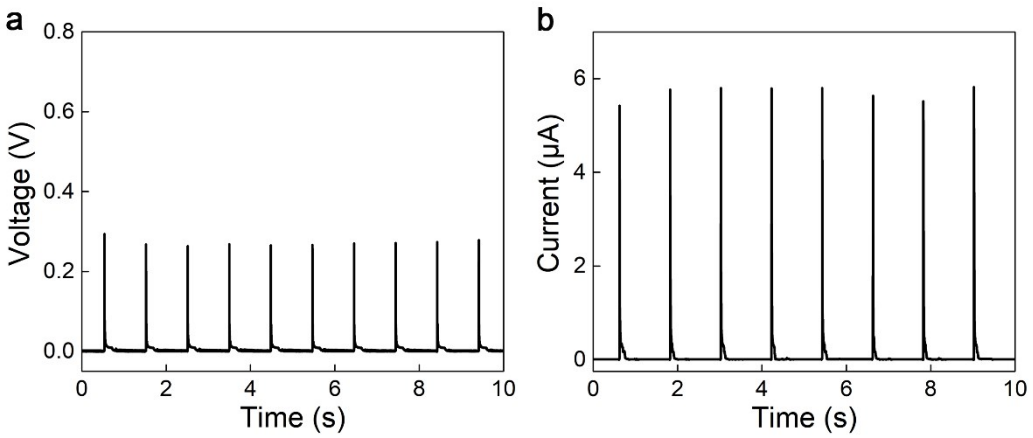

Fig. S12 (a) Voltage and (b) current outputs of Al/PPy-coated Au device when the two components are in continuous contact during the impact.

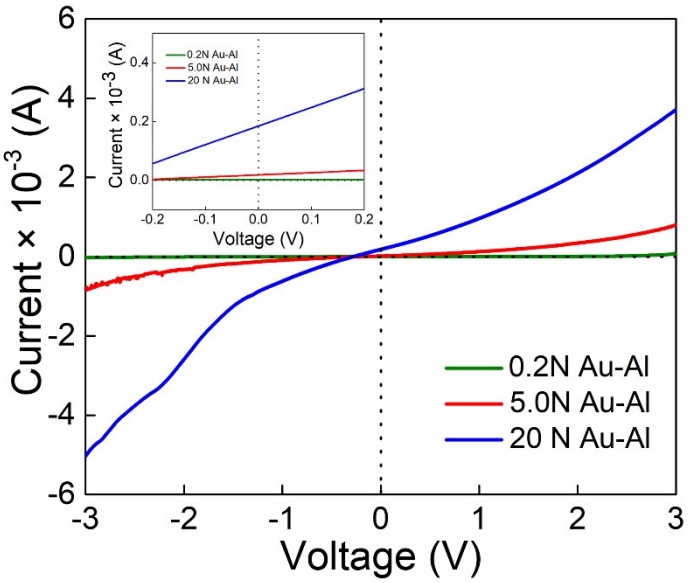

Fig. S13 I-V characteristics of Al/PPy-coated Au at different forces, inset: the enlarged display to show the curves at around the origin point.

The enlarged view indicates that the curves do not pass the origin point, which is an indication of Schottky piezoelectric conversion.

Fig.S14 Temperature of the fabric (a) before and (b) just after 1000 cycles of compression-and-decompression impacts (1 Hz, 13 N).

The accuracy of the thermal imager is 1.5 °C. The temperature difference between the uncompressed and compressed fabric falls into the range of the instrument error.

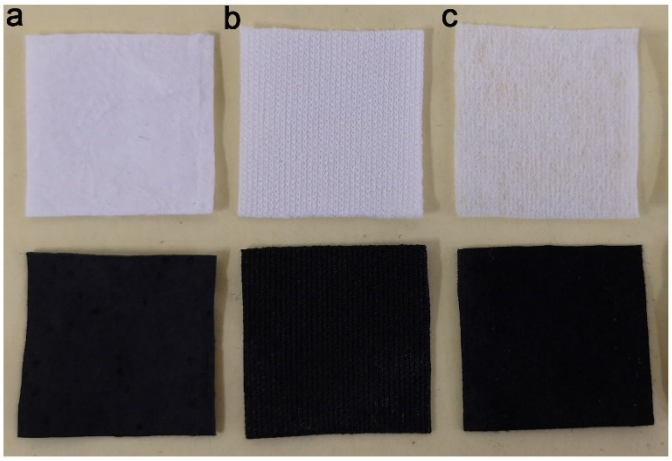

Fig. S15 Pictures to show (a) PP nonwoven, (b) polyester wipers, and (c) cellulose nonwoven fabrics before and after coating with PPy.

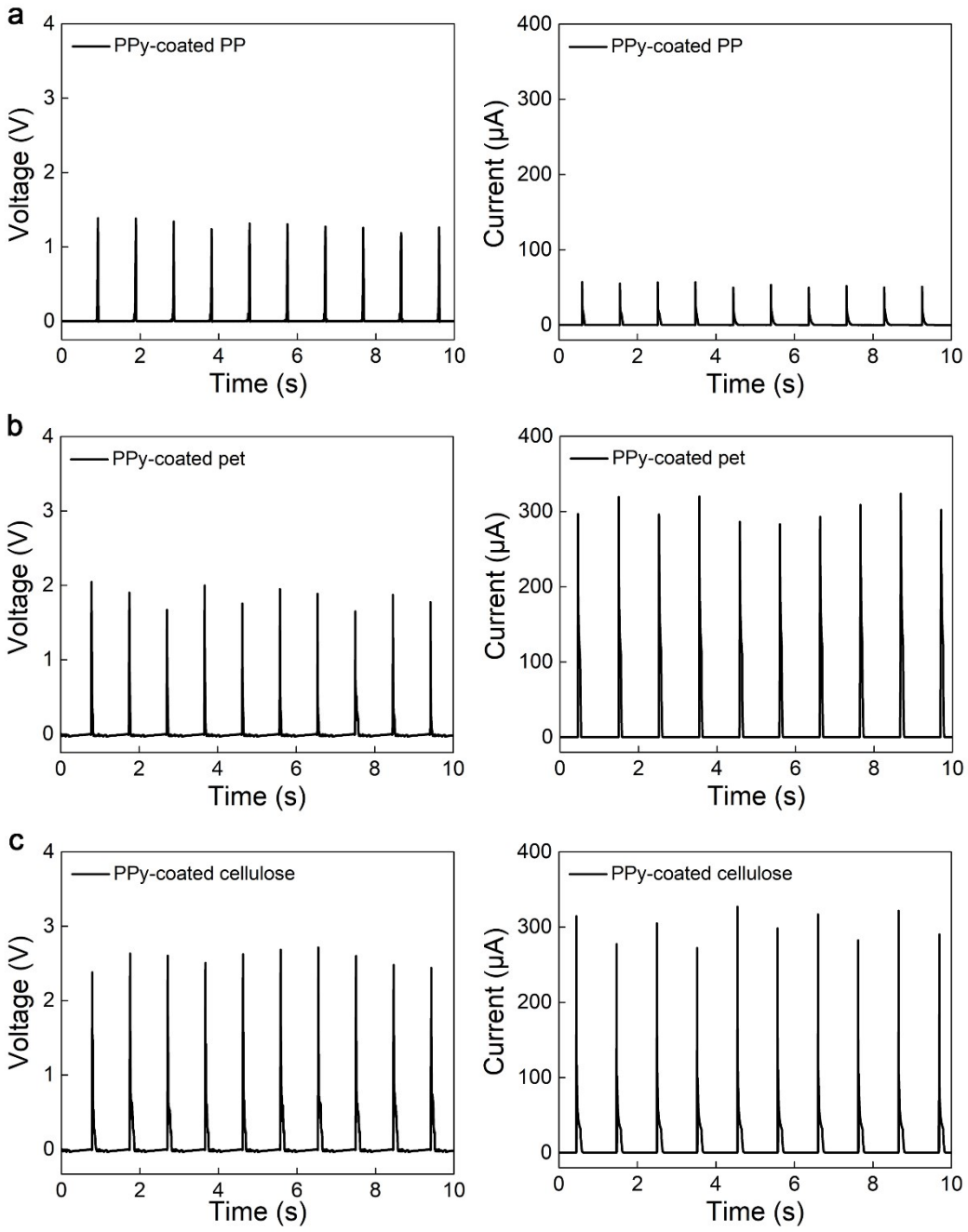

Fig. S16 Electrical outputs of the Al/PPy-coated fabric/Au made of (a) PPy-coated PP fabric, (b) PPy-coated pet fabric, and (c) PPy-coated cellulose fabric.

Table S1 Summary of DC generators

Types	Active layers	Peak Voltage (V)	Current Density ($\mu A/cm^2$)	Refs
piezoelectric	ZnO nanowire array	0.001	2.5×10^{-5}	1
	ZnO nanorod array	-	3.7	2
	Tilted ZnO nanorods	-	0.8	3
	ZnO nanowire-nanowall hybrid	0.02	0.5	4
	ZnO nanotube arrays	0.0001	6.9	5
	ZnO nanosheets-anionic layer	0.75	16	6
	Vanadiun-doped ZnO nanosheet	-	1	7
	ZnO nanosheets-Zn:Al layered double	0.38	22.1	8
	Hydroxide layer ZnO-NiO	0.43	0.04	9
	Obliquely aligned InN nanowire array	7×10^{-4}	4.5	10
	DI water-Graphene PVDF heterostructure	0.0155	-	11
	DI water-Graphene SiO_2/Si heterosture	0.000028	-	11
	DI water-Graphene $LiNbO_3$ heterostructure	0.00011	-	11
Triboelectric	Al-PVC	-	0.4	12
	Al-rubber-PTFE **(**phase exchange via mechanical unit**)**	3200	(20 μA, no area found)	13
	MoS_2-Pt/Ir coated AFM tip	-	10^8	14
	p-n junction charge regulated device	-	14.7	15
	Al-FEP	-	4.1	16
	PTFE-MC nylon	380	0.36	17
	P type Si-Pt/Ir coated AFM tip	0.4	10^6	18
	N-type Si/P-type Si	0.425	0.58	19
	FEP-Cu (using DI water as a mobile phase)	228	(11.5 μA, no area found)	20
	FEP-Cu (using copper pellets as the mobile phase)	101	(1.35 μA, no area found)	20
	Copper-PTFE (sliding mode)	14.2	0.39 (1.05μA, PTFE area: 3 cm×9 mm)	21

	Copper-PTFE (rotary mode)	750	(15 μA, no area found)	21
	Al-MoS_2	0.3	35	22
	Ti/Si wafer-TiO_2-MoS_2	-0.7	120	22
	N-type diamond coated tip and ICP-RIE treated p type Si	-	(55 pA, no area found)	23
	Pt coated tip and the ICP-RIE treated N type Si	-	(-2000 pA, no area found)	23
	BMP/PTFE	1300	1.05	24
	PA conductive yarn-PA nonconductive yarn-PTFE	4500	0.84 (40 μA, area: 6.8 cm×7 cm)	25
	Copper foil-Kapton film (sliding DC-TENG)	-	0.04 (0.16 μA, area: 2 cm×2 cm)	26
	n-type doped Si/stainless heterostructure	0.02	9 (18 μA, area: 2cm^2)	27
	Cu-FEP	480	(12 μA, no area found)	28
Radiofrequency harvesters from Schottky diode	MoS_2 phase-junction	3.5	-	36
	Graphene/GaAs	0.00008	(10^{-8}-10^{-7} A, no area found)	37
	Graphene/Al_2O_3/Si	0.0013	(0.2 μA, no area found)	37
	Graphene/AIN/Si	0.0015	(0.25μA, no area found)	37
Schottky diode/p-n junction (Sliding mode)	Al tip/N-type Si	0.60	4000	29
	Graphene/N-type Si	0.22	1.5	29, 30
	ITO/N-type Si	0.45	2.5	29, 30
	Al/N-type Si	0.60	4	29, 30
	Graphene/N-GaAs	0.12	0.14	29
	ITO/N-GaAs	0.23	0.25	29
	Al/N-GaAs	0.48	4.1	29
	N-GaAs/SiO_2/P-Si	3.1	100	31
	MoS_2/AlN/Si	5.1	11200	31
	P-Si/N-GaAs	0.7	180	31
Schottky diode/p-n junction (Compression mode)	Al/PPy/Au	0.70	62.4	32
	Al/PANI/Au	1.0	33.6	32
	Al/PEDOT/Au	0.87	49.0	32
	Al/PANI-HCl/Au	0.90	33.9	33
	Al/PPy-SnO_2/Au	0.25	2.7	34
	Al/SnO_2/Au	0.08	0.38	34

	Al/PPy-Al_2O_3/Au	0.006	0.004	34
	Al/PPy-ZnO/Au	0.019	0.013	34
	Al/PANI-SnO_2/Au	0.14	0.47	34
	Al/PEDOT-SnO_2/Au	0.1	1.28	34
	Al/PPy-GO/Au	0.73	131.9	35
	Al/PPy-MWCNT/Au	-	10.7	35
	Al/PPy-graphene/Au	-	7.9	35
	Al/PANI-GO/Au	-	10.41	35
	Al-PEDOT-GO/Au	-	10.93	35
	Al/PPy-coated fabric/Au	**3.27**	**82.42**	**This work**

Table S2 Physical properties of PPy-coated fabrics

$FeCl_3$	PPy loading (mg/cm^2)	Areal density (g/m^2)	Surface resistance ($k\Omega/\square$)
0.5 M	2.70	94.74	153.56
1.0 M	4.06	106.92	135.27
1.5 M	4.22	112.52	9.09
2.0 M	6.36	131.53	5.48
2.5 M	6.44	134.33	2.99

Table S3 Physical properties of materials fabrics

Materials	Weight (g/m^2)	Thickness (mm)
PP	40	0.32
Polyester	160	0.57
Cellulose	45	0.30
Polyester/cellulose	65	0.27

Supplementary Videos

Video 1: Running an LCD.

Reference

S-1. X. Wang, J. Song, J. Liu and Z. L. Wang, *Science*, 2007, **316**, 102-105.

S-2. M.-Y. Choi, D. Choi, M.-J. Jin, I. Kim, S.-H. Kim, J.-Y. Choi, S. Y. Lee, J. M. Kim and S.-W. Kim, *Adv. Mater.*, 2009, **21**, 2185-2189.

S-3. H.-K. Park, K. Y. Lee, J.-S. Seo, J.-A. Jeong, H.-K. Kim, D. Choi and S.-W. Kim, *Adv. Funct. Mater.*, 2011, **21**, 1187-1193.

S-4. B. Kumar, K. Y. Lee, H.-K. Park, S. J. Chae, Y. H. Lee and S.-W. Kim, *ACS Nano*, 2011, **5**, 4197-4204.

S-5. Y. Xi, D. H. Lien, R. S. Yang, C. Xu and C. G. Hu, *Physica Status Solidi-Rapid Research Letters*, 2011, **5**, 77-79.

S-6. K.-H. Kim, B. Kumar, K. Y. Lee, H.-K. Park, J.-H. Lee, H. H. Lee, H. Jun, D. Lee and S.-W. Kim, *Sci. Rep.*, 2013, **3**.

S-7. M. K. Gupta, J.-H. Lee, K. Y. Lee and S.-W. Kim, *ACS Nano*, 2013, **7**, 8932-8939.

S-8. G. C. Yoon, K.-S. Shin, M. K. Gupta, K. Y. Lee, J.-H. Lee, Z. L. Wang and S.-W. Kim, *Nano Energy*, 2015, **12**, 547-555.

S-9. B. Yin, Y. Qiu, H. Zhang, J. Lei, Y. Chang, J. Ji, Y. Luo, Y. Zhao and L. Hu, *Nano Energy*, 2015, **14**, 95-101.

S-10. N.-J. Ku, G. Liu, C.-H. Wang, K. Gupta, W.-S. Liao, D. Ban and C.-P. Liu, *Nanoscale*, 2017, **9**, 14039-14046.

S-11. H. Zhong, J. Xia, F. Wang, H. Chen, H. Wu and S. Lin, *Adv. Funct. Mater.*, 2017, **27**, 1604226.

S-12. C. Zhang, T. Zhou, W. Tang, C. Han, L. Zhang and Z. L. Wang, *Advanced Energy Materials*, 2014, **4**, 1301798.

S-13. Y. Yang, H. Zhang and Z. L. Wang, *Adv. Funct. Mater.*, 2014, **24**, 3745-3750.

S-14. J. Liu, A. Goswami, K. Jiang, F. Khan, S. Kim, R. McGee, Z. Li, Z. Hu, J. Lee and T. Thundat, *Nature Nanotechnology*, 2018, **13**, 112-116.

S-15. X. S. Meng, Z. L. Wang and G. Zhu, *Adv. Mater.*, 2016, **28**, 668-676.

S-16. J. Luo, L. Xu, W. Tang, T. Jiang, F. R. Fan, Y. Pang, L. Chen, Y. Zhang and Z. L. Wang, *Advanced Energy Materials*, 2018, **8**, 1800889.

S-17. H. Ryu, J. H. Lee, U. Khan, S. S. Kwak, R. Hinchet and S.-W. Kim, *Energy Environ. Sci.*, 2018, **11**.

S-18. J. Liu, M. Miao, K. Jiang, F. Khan, A. Goswami, R. McGee, Z. Li, N. Lan, Z. Hu, J. Lee, K. Cadien and T. Thundat, *Nano Energy*, 2018, **48**, 320-326.

S-19. R. Xu, Q. Zhang, J. Y. Wang, D. Liu, J. Wang and Z. L. Wang, *Nano Energy*, 2019, **66**, 104185.

S-20. J. Wang, Z. Wu, L. Pan, R. Gao, B. Zhang, L. Yang, H. Guo, R. Liao and Z. L. Wang, *Acs Nano*, 2019, **13**, 2587-2598.

S-21. D. Liu, X. Yin, H. Guo, L. Zhou, X. Li, C. Zhang, J. Wang and Z. L. Wang, *Science Advances*, 2019, **5**.

S-22. J. Liu, F. Liu, R. Bao, K. Jiang, F. Khan, Z. Li, H. Peng, J. Chen, A. Alodhayb and T. Thundat, *Acs Applied Materials & Interfaces*, 2019, **11**, 35404-35409.

S-23. M. Zheng, S. Lin, L. Xu, L. Zhu and Z. L. Wang, *Adv. Mater.*, 2020, **32**, 2000928.

S-24. H.-J. Yoon, M. Kang, W. Seung, S. S. Kwak, J. Kim, H. T. Kim and S.-W. Kim, *Advanced Energy Materials*, 2020, **10**.

S-25. C. Chen, H. Guo, L. Chen, Y.-C. Wang, X. Pu, W. Yu, F. Wang, Z. Du and Z. L. Wang, *Acs Nano*, 2020, **14**, 4585-4594.

S-26. L. Zhou, D. Liu, Z. Zhao, S. Li, Y. Liu, L. Liu, Y. Gao, Z. L. Wang and J. Wang, **n/a**, 2002920.

S-27. Z. Zhang, D. Jiang, J. Zhao, G. Liu, T. Bu, C. Zhang and Z. L. Wang, 2020, **10**, 1903713.
S-28. G. Qiao, J. Wang, X. Yu, R. Jia, T. Cheng and Z. L. Wang, *Nano Energy*, 2021, **79**, 105408.
S-29. S. Lin, Y. Lu, S. Feng, Z. Hao and Y. Yan, *Adv. Mater.*, 2019, **31**, 1804398.
S-30. S. Lin, Y. Lu, S. Feng, Z. Hao and Y. Yan, *Adv. Mater*, 2018, **2019**, 1804398.
S-31. Y. Lu, S. Feng, Z. Hao, R. Shen and S. Lin, *iScience*, 2019, **22**, 58-69.
S-32. H. Shao, J. Fang, H. Wang, L. Dai and T. Lin, *Adv. Mater.*, 2016, **28**, 1461-1466.
S-33. H. Shao, J. Fang, H. Wang, H. Zhou, H. Niu, F. Chen, G. Yan, S. Fu, Y. Cao and T. Lin, *Advanced Electronic Materials*, 2019, **5**, 1800675.
S-34. H. Shao, J. Fang, H. Wang, H. Zhou and T. Lin, *Journal of Materials Chemistry A*, 2017, **5**, 8267-8273.
S-35. H. Shao, J. Fang, H. Wang, H. Niu, H. Zhou, Y. Cao, F. Chen, S. Fu and T. Lin, *Nano Energy*, 2019, **62**, 171-180.
S-36. X. Zhang, J. Grajal, J. Luis Vazquez-Roy, U. Radhakrishna, X. Wang, W. Chern, L. Zhou, Y. Lin, P.-C. Shen, X. Ji, X. Ling, A. Zubair, Y. Zhang, H. Wang, M. Dubey, J. Kong, M. Dresselhaus and T. Palacios, *Nature*, 2019, **566**, 368-372.
S-37. Y. Xuan, H. Chen, Y. Chen, H. Zheng, Y. Lu and S. Lin, *Research*, 2020, **2020**, 3850389-3850389.